Anharmonic Origin of Giant Thermal Displacements in the Metal-Organic Framework UiO-67

Katrine L. Svane,[†] Jessica K. Bristow,[†] and Aron Walsh[*,‡,¶]

†*Department of Chemistry, University of Bath, Bath BA2 7AY, United Kingdom*

‡*Department of Materials, Imperial College London, London SW7 2AZ, United Kingdom*

¶*Department of Materials Science and Engineering, Yonsei University, Seoul 120-749, Korea*

E-mail: a.walsh@imperial.ac.uk

Abstract

The crystallography of mechanically soft materials such as hybrid organic-inorganic compounds often reveals large thermal displacement factors and partially occupied lattice sites, which can arise from static or dynamic disorder. A combination of *ab initio* lattice dynamics and molecular dynamics simulations reveals the origin of the giant thermal displacements in the biphenyl-4,4'-dicarboxylate (BPDC) linker in the metal-organic framework UiO-67. The dihedral angle between the two phenyl rings has two equivalent minima at $\pm 31°$, which cannot be described by harmonic phonons. Instead, anharmonic switching between the minima results in the experimentally observed large thermal ellipsoids. The switching frequency is found to be similar in the topologically distinct framework IRMOF-10, suggesting that dynamic disorder is a general feature of MOFs based on BPDC and structurally similar linkers.

Introduction

Metal-organic frameworks (MOFs) are crystalline porous solids formed by the combination of a metal and an organic linker, and the void space within the pores have made them highly interesting for applications such as gas storage and catalysis.[1–3] Furthermore the pores are tuneable because substitution of structually similar ligands often results in a topologically identical crystal, which can however have different pore sizes,[4,5] or differ in macroscopic properties such as light adsorption[6,7] or response to pressure.[8]

Being mechanically softer than typical dense inorganic materials, MOFs are prone to structural disorder.[9] This can be static in nature, e.g. arising from structural units occupying one of several equivalent sites with random ordering throughout the crystal, or dynamic, e.g. arising from the thermally activated switching of units between energetically similar sites. Techniques that probe the average structure, such as X-ray diffraction, can not distinguish between these two types of behaviour. Due to the mechanical softness, interesting dynamics can be observed already at low temperatures, with possible consequences for the material

properties and potential applications. Examples include the ferroelectric ordering in some organic-inorganic perovskites, which is lost at higher temperatures due to the thermal motion of the atoms,[10–13] and the negative thermal expansion observed for a number of MOFs.[14–17]

In experimentally determined crystal structures the structural disorder is evidenced by the existence of partial occupancy and large thermal displacement parameters. As an example the biphenyl-4,4'-dicarboxylate (BPDC, see Figure 1a) organic linker in crystal structures of the metal-organic framework UiO-67[4] can be represented in a planar conformation with a dihedral angle (α in Fig. 1a) of 0° between the two phenyl rings and large anisotropic thermal ellipsoids, or in a nonplanar conformation with two partially occupied sites with $\alpha \neq 0$. Structural optimisation of the BPDC linker in IRMOF-10[5] using density functional theory (DFT) found an equilibrium dihedral angle of $\alpha = \pm 30 - 31°$,[18] confirming the preference for a nonplanar geometry in this material. Furthermore this is in agreement with previous calculations of the isolated carboxylic acid.[19,20] However, diffraction data does not reveal if the split occupancy appears as a result of static disorder, i.e. a disordered distribution of linker orientations throughout the crystal, or dynamic disorder, i.e. the dynamical switching of individual linkers between the two equilibrium positions. The dynamic behavior of UiO-67 has previously been simulated, showing large thermal displacements of the ligand atoms, but the details of the ring torsion and mechanism of disorder was not addressed.[8,20]

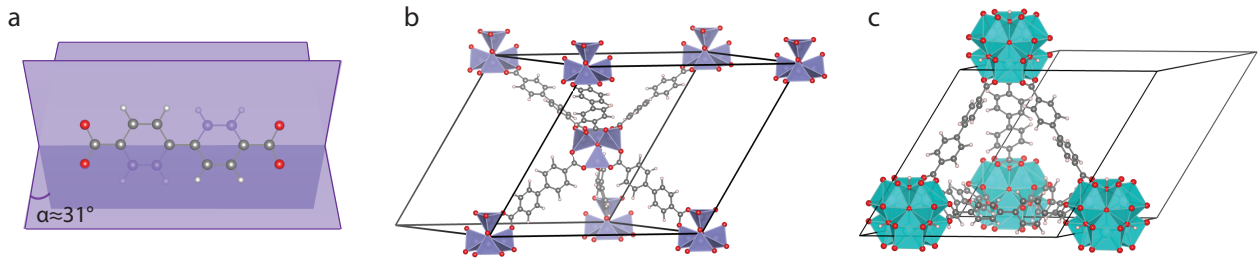

Figure 1: a) Structure of the biphenyl-4,4'-dicarboxylate (BPDC) ligand. The planes indicate the planes of the phenyl rings and shaded atoms are behind one of these planes. The angle between the planes, α, is marked is marked. b-c) primitive unit cells of b) IRMOF-10 and c) UiO-67. Hydrogen is white, oxygen red, carbon grey, zirconium cyan and zinc purple.

In this study, we use a combination of *ab initio* molecular dynamics (MD) simulations and DFT-based phonon calculations to investigate the dynamic behaviour of the BPDC linkers in UiO-67. The MD simulations show that the linkers rotate between the two equilibrium positions at room temperature. The vibrational calculations confirm that the average structure reported experimentally is a saddle point on the potential energy surface. Imaginary harmonic phonon modes are found that correspond to phenyl ring rotations in an anharmonic double well potential. The time constant for the oscillation is found to be ~ 2 ps with an energy barrier of ~ 40 meV. Similar behaviour is also found for IRMOF-10.

Results and Discussion

The crystal structures of UiO-67 and IRMOF-10 were optimised in the primitive unit cell shown in Figure 1b-c using the PBEsol[21] exchange-correlation functional and the D3 correction[22,23] to account for dispersion interactions. Initial geometry optimisation is performed with a plane-wave energy cutoff of 600eV, while the MD simulations are performed with a cutoff of 400eV to lower the computational overhead. A discussion of the accuracy expected from this choice of cutoff is given in the Electronic Supplementary Information (ESI) along with computational details on the setup of the DFT, lattice dynamic, and molecular dynamics calculations.

For IRMOF-10 initial optimisation was performed in the crystallographically determined spacegroup $Fm\bar{3}m$. The resulting structure had imaginary phonon frequencies for modes corresponding to the rotation of the phenyl rings, as these degrees of freedom could not be optimised within the chosen spacegroup. Following the eigenvectors of the imaginary phonons led to a twisting of the rings, and the final structure has no imaginary phonon modes, indicating that it is a local minimum (See the phonon partial density of states in Figure S1 in the ESI). This highlights the importance of phonon calculations to verify that the optimised structure is a true local minimum, in particular when the optimisation

is restricted by symmetry. We note that displacing the structural coordinates along the phonon eigenvectors leads to a loss of crystal symmetry. The final spacegroup for the static structure is formally $P1$ due to small variations in lattice vectors and atomic positions (c.f. ESI for details).

For UiO-67 we model the structure with the hydroxylated metal cluster $Zr_6O_4(OH)_4$ as reported in Ref. 24. The initial structure was created from an experimental structure with nonplanar ligands and partial occupation of the CH groups in the phenyl rings as well as the oxygens and hydroxyl groups of the metal cluster. Due to the initial choice of one of the two partially occupied sites, the optimised structure has a lower symmetry ($F23$) than the crystallographic spacegroup ($Fm\bar{3}m$). The calculated phonon spectrum has no imaginary modes, indicating that the BPDC linker also prefers a nonplanar configuration in this case.

In both optimised structures the dihedral angle between the two phenyl rings is found to be 31° and the calculated lattice constants are in good agreement with the experimentally determined values at room temperature (see Table S2 in the ESI).

To identify whether the observed partial occupancy arises from static or dynamic disorder we performed constant volume MD simulations (NVT ensemble). To determine the appropriate unit cell size for these simulations we compare the thermal displacement parameters extracted for the $1 \times 1 \times 1$ and $2 \times 1 \times 1$ unit cells, following the procedure in Ref. 11, with experimental results. Furthermore, we compared the time constants for the switching process in the two unit cells. From this we decide that a $2 \times 1 \times 1$ supercell (2 metal clusters and 12 linkers) gives a more realistic description of the dynamics in UiO-67 than a $1 \times 1 \times 1$ unit cell, while for IRMOF-10 a $1 \times 1 \times 1$ unit cell (2 metal clusters and 6 linkers) is sufficient (see ESI for simulation details and comparison of different unit cell sizes). Enlarging the supercell expansion of UiO-67 may be necessary for full convergence, but is beyond our computational resources for MD simulations. We expect the increased flexibility of a larger supercell would lead to a small decrease in the energy barriers and time constants derived below, and they can thus be considered upper limits to the true behaviour.

We obtain the time constant for the ring rotation from the simulations by extracting the dihedral angle between the phenyl groups of each of the linkers in the unit cell as a function of time. An example for one of the linkers in UiO-67 is shown in Figure 2. The plot shows that the dihedral angle mostly oscillates around the equilibrium value of $\pm 31°$, with occasional crossings through the planar configuration with a dihedral angle of $0°$. We define a proper transition between the two minima as an event where the dihedral angle changes from a positive value above $10°$ to a negative value below $-10°$ or vice versa. The graph shown in Figure 2 thus shows three proper crossings during the simulation time. Counting the number of crossings for all ligands in the unit cell leads to the averaged time between transitions, τ, which can be converted to the frequency, ν, both given in Table 1.

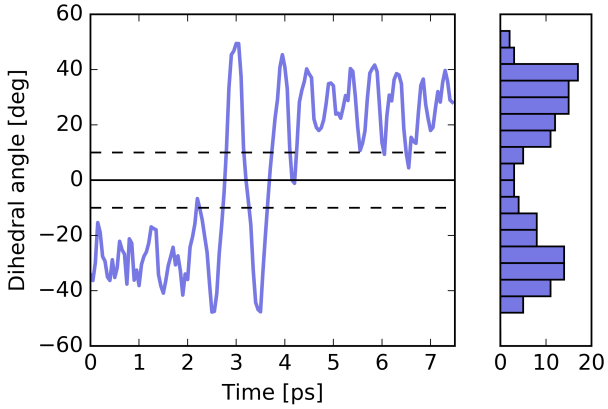

Figure 2: Dihedral angle between the phenyl rings of one molecule as a function of time, with a time resolution of 50 fs. The dashed lines are used to identify a proper crossing and the histogram on the right shows the distribution of angles.

The smaller oscillations around the equilibrium positions most clearly seen in the right part of Figure 2 indicates the vibrational frequency associated with the torsion of the rings, ν_0, which can be considered an attempt frequency for the proper transition. From the simulations we estimate this frequency as an average from several molecules where periodic oscillations are clearly seen. Alternatively, we can identify the phonon modes which are involved in the ring torsion by calculating the change in dihedral angle between the phenyl rings when following the phonon eigenvectors. This procedure identifies six modes with

frequencies of 2.36–2.39 THz as leading to a significant change in dihedral angle in UiO-67, while for IRMOF-10 we find nine modes in the range 2.28–2.56 THz (see animations in the ESI). These ring torsion frequencies are close to those estimated from the MD simulation (c.f. Table 1). For both materials a number of other phonons with frequencies in the range 12–30 THz change the dihedral angle; however, these modes also involve other distortions of the molecules (selected examples are given in the ESI).

Table 1: Average time for the transition between the two local minima, τ, the corresponding frequency, ν, as well as the attempt frequency estimated from the molecular dynamics (MD) simulation and from lattice dynamics (LD), ν_0, and the corresponding energy barriers, E_a.

	UiO-67	IRMOF-10
τ [ps]	1.9	2.4
ν [THz]	0.5	0.4
ν_0 (MD) [THz]	1.9	2.2
ν_0 (LD) [THz]	2.4	2.3
E_a (MD)[meV]	38	36
E_a (LD)[meV]	44	38

Taking the ring-torsion vibrational mode ν_0 as an attempt frequency we can estimate the barrier for the transition (E_a) with the formula:

$$E_a = RT \log(\nu_0/\nu) \tag{1}$$

Where R is the gas constant, T is the temperature and ν is the frequency of the proper crossings. The results are given in Table 1, using the two different attempt frequencies obtained directly from the MD simulations and from the phonon calculations, respectively. The switching barrier is similar in the two materials in spite of their different topologies. Our simulation accuracy is not sufficient to distinguish between them, but difference could be expected due to changes in connectivity, stiffness, or the interaction between neighbouring linkers. The low barrier for switching combined with the high attempt frequency indicates that it will occur at all technologically relevant temperatures, with possible implications for the material properties. Structural dynamics has been shown to affect the interaction

between adsorbed molecules and the linkers[25] and we will show in the following that it can also affect the electronic structure.

To further investigate the energy landscape for the process we calculate the energy for different dihedral angles for an isolated BPDC linker (cf. ESI for computational details). Calculations for the neutral carboxylic acid and the negatively charged dianion versions of the BPDC linker reveal very similar curves (cf. ESI) and we therefore show the results for the protonated molecule only (Figure 3), with the carboxylic acid groups left free to rotate (full line) or fixed in a plane (dashed line). The latter situation mimicks a strongly directional bond between the carboxylic acid group and the metal cluster in the MOF; the real system probably provides a less rigid constraint on the orientation. A polynomial fit to the calculated energies shows that the minimum energy is found at an angle of approximately 30° in reasonable agreement with the 45° previously obtained with the Hartree-Fock method[19] and the 30° obtained with hybrid DFT.[20] The difference in energy between the minima of the double well and the transition state at 0° is calculated to be 52 meV and 30 meV for the free and constrained carboxylic acid groups, respectively, corresponding well with the values calculated from the MD simulations and previous calculations of the rotational barrier in biphenyl.[26] As hybrid functionals are known to provide a better description of molecular geometries the present calculations were also performed with the PBE0 functional,[27] which showed qualitatively similar results but slightly larger values for the energy barrier (39-77 meV) and the optimal torsion angle (28°-38°, c.f. ESI).

Looking at the electronic structure, the DFT one-electron eigenvalues either increase, decrease or remain constant when going from 0° to 60°, depending on whether the interaction across the bond connecting the phenyl rings is bonding, anti-bonding or non-bonding. The highest occupied molecular orbital (HOMO, see Figure S3) increases in energy when the angle goes towards 0°, while the lowest unoccupied molecular orbital (LUMO, see Figure S3) decreases in energy, and the HOMO-LUMO gap at 0° is thus 0.17 eV smaller than at the optimum angle for the neutral molecule (0.30 eV with PBE0). Since the highest occupied

and lowest unoccupied crystalline orbitals in UiO-67 primarily consist of the HOMO and LUMO of the isolated linkers (c.f. Figure S3 in the ESI), this particular motion would be expected to lead to large thermal fluctuations and a decrease in the average band gap of UiO-67, however calculations of the total effect of electron-phonon coupling in UiO-67 based on time-dependent DFT show a much smaller change in the excitation energy of 24 meV.[20]

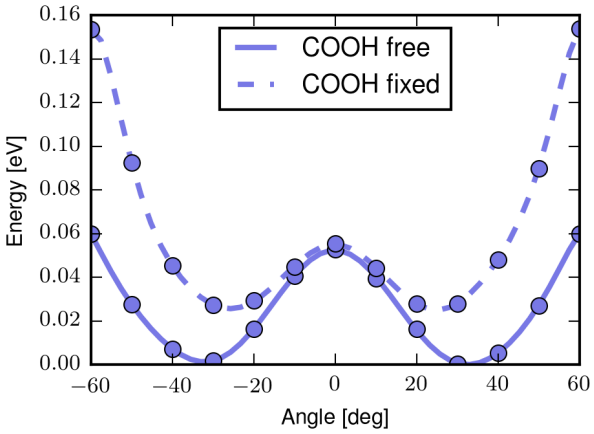

Figure 3: Potential energy as a function of the dihedral angles for the isolated BPDC linker capped by hydrogen with the carboxylic acid group fixed in a plane (dashed line) or free to rotate (full line). The saddle point at 0° corresponds to the average structure of the ligand that is seen from X-ray diffraction experiments.

Conclusion

In conclusion we have investigated the origin of the large thermal displacements of the organic BPDC linker in the MOFs UiO-67 and IRMOF-10. We identify the equilibrium local-minumum structure of the two materials as having a dihedral angle of ±31°. We calculate the underlying double-well potential and show that switching between the two wells happens on the picosecond time scale at room temperature. The calculated energy barrier for this process is similar in the two materials, suggesting that switching is largely independent of the nature and connectivity of the metal clusters, and thus would be found in other MOFs containing this particular ligand, or ligands of the same family. This should be considered

in the crystallographic refinement procedures and computational structure optimisation as the properties of the static average structure are different from the true dynamic system.

Acknowledgement

K. L. S. is funded by ERC programme grant no. 277757 and J. K. B. is funded by the EPSRC (grant no. EP/G03768X/1). The authors acknowledge computing support from the UK national supercomputing service (Archer), via membership of the UK Materials Chemistry Consortium which is funded by EPSRC (EP/L000202), and from the University of Bath computing services (Balena).

Supporting Information Available

Electronic Supplementary Information (ESI): Optimised structures, phonon calculation output, gifs of selected phonon modes and MD trajectories are available from [link inserted after acceptance]. Details of structural optimisation and MD simulations, comparison of thermal displacement data and additional calculations of the isolated linker.

References

(1) Ma, S.; Zhou, H.-C. Gas storage in porous metal-organic frameworks for clean energy applications. *Chem. Commun.* **2010**, *46*, 44–53.

(2) Lee, J.; Farha, O. K.; Roberts, J.; Scheidt, K. A.; Nguyen, S. T.; Hupp, J. T. Metal-organic framework materials as catalysts. *Chem. Soc. Rev.* **2009**, *38*, 1450–1459.

(3) Wilmer, C. E.; Leaf, M.; Lee, C. Y.; Farha, O. K.; Hauser, B. G.; Hupp, J. T.; Snurr, R. Q. Large-scale screening of hypothetical metal–organic frameworks. *Nature Chem.* **2012**, *4*, 83–89.

(4) Cavka, J. H.; Jakobsen, S.; Olsbye, U.; Guillou, N.; Lamberti, C.; Bordiga, S.; Lillerud, K. P. A new zirconium inorganic building brick forming metal organic frameworks with exceptional stability. *J. Am. Chem. Soc.* **2008**, *130*, 13850–13851.

(5) Eddaoudi, M.; Kim, J.; Rosi, N.; Vodak, D.; Wachter, J.; O'Keeffe, M.; Yaghi, O. M. Systematic design of pore size and functionality in isoreticular MOFs and their application in methane storage. *Science* **2002**, *295*, 469–472.

(6) Hendon, C. H.; Tiana, D.; Fontecave, M.; Sanchez, C.; D'arras, L.; Sassoye, C.; Rozes, L.; Mellot-Draznieks, C.; Walsh, A. Engineering the optical response of the titanium-MIL-125 metal-organic framework through ligand functionalization. *Journal of the American Chemical Society* **2013**, *135*, 10942–10945.

(7) Spoerke, E. D.; Small, L. J.; Foster, M. E.; Wheeler, J.; Ullman, A. M.; Stavila, V.; Rodriguez, M.; Allendorf, M. D. MOF-sensitized solar cells enabled by a pillared porphyrin framework. *J. Phys. Chem. C.* **2017**, *121*, 4816–4824.

(8) Hobday, C. L.; Marshall, R. J.; Murphie, C. F.; Sotelo, J.; Richards, T.; Allan, D. R.; Düren, T.; Coudert, F.-X.; Forgan, R. S.; Morrison, C. A. et al. A computational and experimental approach linking disorder, high-pressure behavior, and mechanical properties in UiO frameworks. *Angew. Chemie* **2016**, *128*, 2447–2451.

(9) Cairns, A. B.; Goodwin, A. L. Structural disorder in molecular framework materials. *Chem. Soc. Rev.* **2013**, *42*, 4881–4893.

(10) Chen, S.; Shang, R.; Hu, K.-L.; Wang, Z.-M.; Gao, S. $[NH_2NH_3][M(HCOO)_3]$ (M = Mn^{2+}, Zn^{2+}, Co^{2+} and Mg^{2+}): structural phase transitions, prominent dielectric anomalies and negative thermal expansion, and magnetic ordering. *Inorg. Chem. Front.* **2014**, *1*, 83–98.

(11) Svane, K. L.; Walsh, A. Quantifying thermal disorder in metal-organic frameworks:

Lattice dynamics and molecular dynamics simulations of hybrid formate perovskites. *J. Phys. Chem. C* **2017**, *121*, 421–429.

(12) Gómez-Aguirre, L. C.; Pato-Doldán, B.; Stroppa, A.; Yáñez-Vilar, S.; Bayarjargal, L.; Winkler, B.; Castro-García, S.; Mira, J.; Sánchez-Andújar, M.; Señarís-Rodríguez, M. A. Room-temperature polar order in $[NH_4][Cd(HCOO)_3]$ - A hybrid inorganic-organic compound with a unique perovskite architecture. *Inorg. Chem.* **2015**, *54*, 2109–2116.

(13) Wang, F.-F.; Chen, C.; Zhang, Y.; Ye, H.-Y.; Ye, Q.; Fu, D.-W. A prominent dielectric material with extremely high-temperature and reversible phase transition in the high thermally stable perovskite-like architecture. *J. Mater. Chem. C* **2015**, *3*, 6350–6358.

(14) Goodwin, A. L. Rigid unit modes and intrinsic flexibility in linearly bridged framework structures. *Phys. Rev. B* **2006**, *74*, 134302.

(15) Zhou, W.; Wu, H.; Yildirim, T.; Simpson, J. R.; Walker, A. R. H. Origin of the exceptional negative thermal expansion in metal-organic framework-5 $Zn_4O(1,4-\text{benzenedicarboxylate})_3$. *Phys. Rev. B* **2008**, *78*, 054114.

(16) Han, S. S.; Goddard, W. A. Metal-organic frameworks provide large negative thermal expansion behavior. *J. Phys. Chem. C* **2007**, *111*, 15185–15191.

(17) Cliffe, M. J.; Hill, J. A.; Murray, C. A.; Coudert, F.-X.; Goodwin, A. L. Defect-dependent colossal negative thermal expansion in UiO-66(Hf) metal-organic framework. *Phys. Chem. Chem. Phys.* **2015**, *17*, 11586–11592.

(18) Bristow, J. K.; Skelton, J. M.; Svane, K. L.; Walsh, A.; Gale, J. D. A general forcefield for accurate phonon properties of metal-organic frameworks. *Phys. Chem. Chem. Phys.* **2016**, *18*, 29316–29329.

(19) Matos, M. A. R.; Miranda, M. S.; Martins, D. V. S. S.; Pinto, N. A. B.; Morais, V. M. F.; Liebman, J. F. Thermochemistry of biphenylcarboxylic and dicarboxylic acids. A combined experimental and theoretical study. *Org. Biomol. Chem.* **2004**, *2*, 1353–1358.

(20) Van Yperen-De Deyne, A.; Hendrickx, K.; Vanduyfhuys, L.; Sastre, G.; Van Der Voort, P.; Van Speybroeck, V.; Hemelsoet, K. Vibrational fingerprint of the absorption properties of UiO-type MOF materials. *Theor. Chem. Acc.* **2016**, *135*, 102.

(21) Perdew, J. P.; Ruzsinszky, A.; Csonka, G. I.; Vydrov, O. A.; Scuseria, G. E.; Constantin, L. A.; Zhou, X.; Burke, K. Restoring the density-gradient expansion for exchange in solids and surfaces. *Phys. Rev. Lett.* **2008**, *100*, 136406.

(22) Grimme, S.; Antony, J.; Ehrlich, S.; Krieg, H. A consistent and accurate ab initio parametrization of density functional dispersion correction (DFT-D) for the 94 elements H-Pu. *J. Chem. Phys.* **2010**, *132*, 154104.

(23) Grimme, S.; Ehrlich, S.; Goerigk, L. Effect of the damping function in dispersion corrected density functional theory. *J. Comput. Chem.* **2011**, *32*, 1456–1465.

(24) Øien, S.; Wragg, D.; Reinsch, H.; Svelle, S.; Bordiga, S.; Lamberti, C.; Lillerud, K. P. Detailed structure analysis of atomic positions and defects in zirconium metal-organic frameworks. *Crystal Growth & Design* **2014**, *14*, 5370–5372.

(25) Amirjalayer, S.; Tafipolsky, M.; Schmid, R. Molecular dynamics simulation of benzene diffusion in MOF-5: Importance of lattice dynamics. *Angew. Chem.* **2007**, *46*, 463–466.

(26) Göller, A.; Grummt, U.-W. Torsional barriers in biphenyl, 2,2-bipyridine and 2-phenylpyridine. *Chem. Phys. Lett.* **2000**, *321*, 399 – 405.

(27) Adamo, C.; Barone, V. Toward reliable density functional methods without adjustable parameters: The PBE0 model. *J. Chem. Phys.* **1999**, *110*, 6158–6170.

Graphical TOC Entry